

Identifying Thorne-Żytkow Objects through Neutrinos

PABLO MARTÍNEZ-MIRAVÉ ¹, IRENE TAMBORRA ¹ AND ALEJANDRO VIGNA-GÓMEZ ²

¹*Niels Bohr International Academy and DARK, Niels Bohr Institute, University of Copenhagen, Blegdamsvej 17, 2100, Copenhagen, Denmark*

²*Max Planck Institute for Astrophysics, Karl-Schwarzschild-Strasse 1, 85748, Garching bei München, Germany*

ABSTRACT

Thorne-Żytkow Objects (TŻOs) have been predicted to form when a neutron star is engulfed by a diffuse, convective giant envelope. Accretion onto a neutron star at a rate that is larger than $10^{-4} M_{\odot} \text{ yr}^{-1}$ is expected to lead to significant emission of neutrinos of all flavors with energy of 1–100 MeV. Since the neutrino signal is expected to largely vary in time (from milliseconds to thousands of years), we outline detection strategies tailored to the signal duration. We find that neutrino detection from TŻOs up to the Small Magellanic Cloud is within the reach of current- and next-generation neutrino observatories, such as Super- and Hyper-Kamiokande, the IceCube Neutrino Observatory, and JUNO. Interestingly, if targeted searches for neutrinos from TŻO candidates (e.g. VX Sgr in our Galaxy as well as HV 2112 and HV 11417 in the Small Magellanic Cloud) should lead to positive results, neutrinos could positively identify the nature of such sources and their accretion rate. Our findings should serve as motivation for establishing dedicated searches for neutrino emission from TŻOs. This is especially timely since it is challenging to detect TŻOs via electromagnetic radiation unambiguously, and the TŻO gravitational wave signal could be probed with next-generation detectors for sources within our Galaxy only.

1. INTRODUCTION

Thorne-Żytkow Objects (TŻOs) are stellar bodies characterized by a compact object surrounded by an extended and diffuse envelope (O’Grady et al. 2024). TŻOs are expected to form when a neutron star is engulfed by another star, likely a red giant or supergiant (Thorne & Zytkow 1975, 1977). Potential formation channels of TŻOs include binary coalescence, following a common-envelope phase, and direct collision of the two stellar objects in dense dynamical environments.

As the neutron star pierces through the outer layers of the red supergiant, matter from the red supergiant envelope rapidly accretes onto the central compact core at an hypercritical (super-Eddington) rate, resulting in high-density and temperature regions ($\rho \gtrsim 10^5 \text{ g cm}^{-3}$ and $T \gtrsim 10^{10} \text{ K}$) in the surroundings of the central compact object. If the mass of the latter exceeds the Tolman–Oppenheimer–Volkoff limit, a black hole forms.

Population synthesis models predict $\mathcal{O}(1\text{--}100)$ TŻOs in the Milky Way (Podsiadlowski et al. 1995; Nathaniel et al. 2024). Figure 1 displays a collection of candidates monitored in the Local Group (Kuchner et al. 2002; Levesque et al. 2014; Beasor et al. 2018; Taberner et al. 2021; O’Grady et al. 2023). In addition, as illustrated in Fig. 1, nearby high-mass

X-ray binaries (HMXBs) may undergo unstable mass transfer (Hutchinson-Smith et al. 2024; Ge et al. 2024; Manikantan et al. 2024), potentially leading to the formation of TŻOs. Potential TŻO progenitors can also be found in stellar clusters in the Milky Way, which are rich in red supergiants (DeMarchi et al. 2021).

Due to the high temperature characterizing the core of the newly formed TŻO, thermonuclear reactions can take place; in fact, TŻOs have been considered as production sites of heavy proton-rich isotopes through the rapid proton capture (*rp*) process (Cannon 1993; Nava-Callejas et al. 2024). Observationally, TŻOs are expected to resemble red supergiants, or nitrogen-rich Wolf–Rayet stars (if the star is not stripped of the hydrogen layer), with peculiar spectroscopic lines coming from the synthesis of lithium, rubidium, molybdenum, and calcium (Biehle 1994; Podsiadlowski et al. 1995; Farmer et al. 2023). Since it is challenging to assess the presence of a neutron-star core solely relying on the electromagnetic signatures, a multi-messenger approach involving the detection of gravitational waves from the rotating neutron star or a common-envelope evolution phase has been invoked to allow us for the unambiguous identification of TŻOs (DeMarchi et al. 2021; Nazin & Postnov 1995; DeMarchi et al. 2021; Renzo et al. 2021; Moran-Fraile et al. 2023).

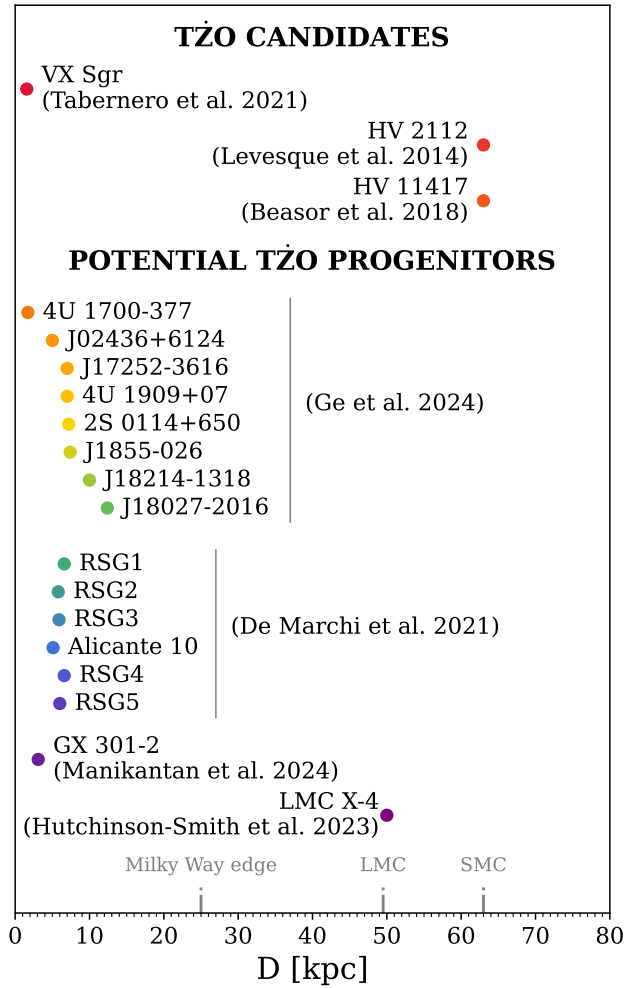


Figure 1. TŻO candidates (Tabernero et al. 2021; Levesque et al. 2014; Beasor et al. 2018) and potential TŻO progenitors in the Galaxy, as well as in the Large Magellanic Cloud (LMC) and in the Small Magellanic Cloud (SMC). Potential candidates are considered to be (i) high-mass X-ray binaries in which the neutron star accretes matter from the stellar companion and unstable mass transfer is expected (Ge et al. 2024; Manikantan et al. 2024; Hutchinson-Smith et al. 2024) and (ii) stellar clusters where red supergiants are abundant (DeMarchi et al. 2021).

In this *Letter*, we propose neutrinos as key messengers to identify these fascinating stellar objects, even with neutrino observatories currently taking data. In fact, for accretion rates ranging from $10^{-4} M_{\odot} \text{ yr}^{-1}$ to $10^6 M_{\odot} \text{ yr}^{-1}$, we estimate that the temperature in the vicinity of the neutron star is $\sim \mathcal{O}(1-10)$ MeV. Such conditions

could lead to the copious production of neutrinos with energy in the 10–100 MeV range¹.

We compute the neutrino emission from TŻOs with accretion rate larger than $10^{-4} M_{\odot} \text{ yr}^{-1}$. We tailor the detection strategy according to the duration of the expected neutrino emission. The inclusion of neutrinos in TŻO searches is especially timely, given that current gravitational wave detectors are not sensitive to these objects. We introduce the source model in § 2 and the thermal neutrino spectral distribution expected from TŻOs in § 3. We then investigate the detection prospects of neutrinos from TŻOs in § 4 in existing and next-generation neutrino observatories and assess the contribution of TŻOs to the diffuse background of astrophysical neutrinos in § 5. We discuss and summarize our findings in § 6. Additional details on the TŻO source model and the neutrino production rates are presented in Appendix A, while Appendix B focuses on the modeling of the expected event rates in neutrino observatories, respectively.

2. SOURCE MODEL

We focus on TŻOs with hypercritical accretion rates from $10^{-4} M_{\odot} \text{ yr}^{-1}$ to $10^6 M_{\odot} \text{ yr}^{-1}$ (i.e. 3×10^{-12} to $3 \times 10^{-2} M_{\odot} \text{ s}^{-1}$, which is 3–13 orders of magnitude larger than the critical, Eddington-limited rate), since for such cases neutrinos are expected to be the primary energy loss channel. For $\dot{M} \simeq 10^{-4} M_{\odot} \text{ yr}^{-1}$, the photon trapping radius is several orders of magnitude larger than the neutron-star radius ($r_{\text{trapping}} \sim 10^4$ km and grows linearly with the accretion rate, see Houck & Chevalier 1991). Hence, neutrino losses are the main cooling mechanism. For $\dot{M} \simeq 10^6 M_{\odot} \text{ yr}^{-1}$, the neutron star collapses into a black hole within a few minutes, halting the formation of a stable TŻO (Fryer et al. 1996).

As detailed in Appendix A, we compute the neutrino emission rates relying on a steady spherically-symmetric source, building on the model presented in Chevalier (1989). This model assumes steady accretion of shocked gas from the envelope onto the neutron star, subsonic velocity of the shocked matter, and that the postshock flow is adiabatic. As a result, the medium temperature and baryon density profiles scale as power laws as functions of the radius in the proximity of the neutron star (i.e., $T(r) \sim r^{-1}$ and $\rho(r) \sim r^{-3}$) with characteristic temperature and baryon density of $T \sim 10^{10}-10^{11}$ K and $\rho \sim 10^5-10^9 \text{ g cm}^{-3}$. We consider a neutron star with a

¹ Notice that for TŻOs with significantly lower accretion rates, e.g. the case of $10^{-8} M_{\odot} \text{ yr}^{-1}$ discussed in Cannon et al. 1992, neutrino production is negligible.

mass of $1.4 M_\odot$ and radius of 10 km (but the density and temperature profiles depend mildly on these choices).

3. NEUTRINO EMISSION

In the region surrounding the central neutron star and extending tens of kilometres outwards, the dominant neutrino emission channel is electron-positron pair annihilation, as illustrated in Appendix A (cf. Fig. 5). In the core of the neutron star, due to the large density, neutrinos are mainly produced thanks to plasmon decay, but are trapped. Other neutrino emission channels such as bremsstrahlung and photoneutrino production negligibly contribute to the expected neutrino flux from TŻOs, as shown in Fig. 5.

For a neutron star of mass M_{NS} and radius r_{NS} , which accretes a mass Δm at a constant rate, we assume that the energy radiated in neutrinos is a fraction of the gain in gravitational energy of the system. Hence, we define the upper limit on the duration of the neutrino signal as the time to black hole formation:

$$\tau \simeq \frac{1}{L_\nu} \frac{GM_{\text{NS}}\Delta m}{r_{\text{NS}}}, \quad (1)$$

where G is the gravitational constant and L_ν is the neutrino luminosity for all flavors. From Eq. 1, we deduce that the duration of the neutrino signal depends on the amount of accreted mass. Note, that τ provides an upper limit on the actual duration of the neutrino emission, since (i) the amount of accreted mass before collapse might be smaller than Δm and (ii) accretion might not be constant for extended periods of time. Hence, hereafter, we denote the duration of the neutrino emission with $\Delta t_\nu \leq \tau$.

If accretion onto the neutron star occurs at a fast rate (i.e., $\dot{M} \geq 10^4 M_\odot \text{ yr}^{-1} \approx 10^{-12} M_\odot \text{ s}^{-1}$), the formation of a TŻO would be halted by the collapse of the neutron star into a black hole (Chevalier 1993; Fryer et al. 1996). In such cases, neutrino emission would cease promptly (hereafter named ‘‘TŻO burst’’ scenario). Otherwise, we expect a steady neutrino emission (‘‘steady TŻO’’ scenario). Table 1 summarizes the upper limit on the duration of the neutrino signal expected for different accretion rates, assuming $\Delta m = 1 M_\odot$.

Figure 2 displays the neutrino flux for all flavors from a TŻO at 5 kpc from Earth. For large accretion rates, the temperature in the innermost regions increases (cf. Fig. 5) and neutrino emission through pair annihilation is significantly enhanced. As a result, the expected neutrino flux is larger, and the peak of the spectrum shifts to higher energies. Note that electron neutrinos and antineutrinos are produced via charged current and neutral current interactions, hence the electron flavors in

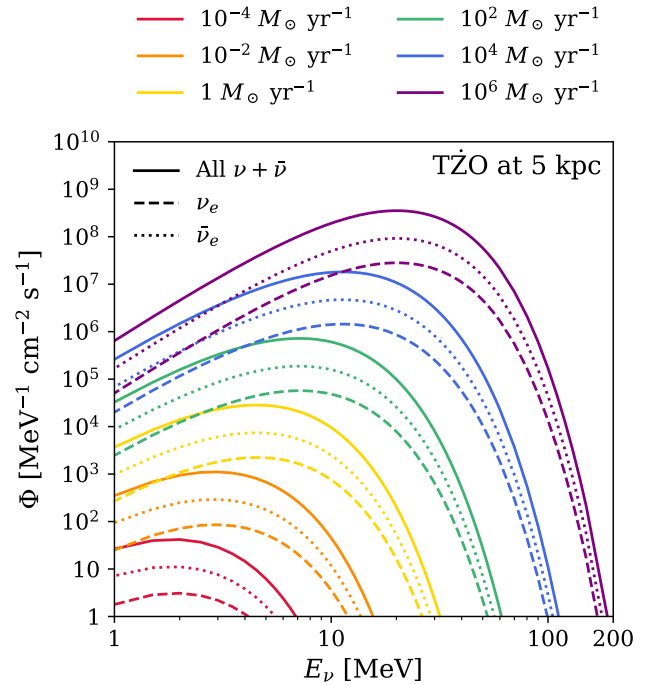


Figure 2. Neutrino flux from a TŻO at 5 kpc from Earth, taking into account flavor conversion. The color lines correspond to the accretion rates considered in this work: $\dot{M} = 10^{-4} M_\odot \text{ yr}^{-1}$, $10^{-2} M_\odot \text{ yr}^{-1}$, $1 M_\odot \text{ yr}^{-1}$, $10^2 M_\odot \text{ yr}^{-1}$, $10^4 M_\odot \text{ yr}^{-1}$, and $10^6 M_\odot \text{ yr}^{-1}$, from bottom to top. Dashed, dotted, and solid lines correspond to electron neutrinos, electron antineutrinos, and the total flux of all neutrinos and antineutrinos, respectively. The neutrino flux increases as a function of the accretion rate, peaking at higher energies.

the production region are more abundant than the non-electron ones (see also dotted and dashed lines in Fig. 2 for $\bar{\nu}_e$ and ν_e , respectively). We stress that, since we rely on a steady TŻO source model, the neutrino emission that we predict is constant over time. In this sense, we provide an upper limit of the expected neutrino flux.

4. NEUTRINO DETECTION PROSPECTS

In the following, we explore the detection prospects of neutrinos from TŻOs in existing and upcoming neutrino observatories. We consider the IceCube Neutrino Observatory, Super-Kamiokande and Hyper-Kamiokande, as well as JUNO. Because of the large variation of the expected duration of the neutrino signal as a function of the accretion rate, we propose tailored detection strategies to enhance the expected sensitivity and distinguish between TŻO bursts (i.e., signal duration $\Delta t_\nu \leq 100$ s and accretion rates $\dot{M} \geq 10^4 M_\odot \text{ yr}^{-1}$) and steady TŻOs

Table 1. Upper limit on the duration of the neutrino signal τ (for $\Delta m = 1M_\odot$, see Eq. 1) and expected neutrino event rates at IceCube, JUNO, Super-Kamiokande, and Hyper-Kamiokande, respectively, from a TŻO at 5 kpc from Earth and for different accretion rates.

| | \dot{M} | τ | IceCube | Super-Kamiokande | JUNO | Hyper-Kamiokande |
|------------|-----------------------------|----------------------|-------------------------------|-------------------------------|-------------------------------|-------------------------------|
| | $[M_\odot \text{ yr}^{-1}]$ | [s] | Signal rate $[\text{s}^{-1}]$ | Signal rate $[\text{s}^{-1}]$ | Signal rate $[\text{s}^{-1}]$ | Signal rate $[\text{s}^{-1}]$ |
| Steady TŻO | 10^{-4} | 1.8×10^{11} | - | $\sim \mathcal{O}(10^{-10})$ | $\sim \mathcal{O}(10^{-11})$ | $\sim \mathcal{O}(10^{-9})$ |
| | 10^{-2} | 2.7×10^9 | - | 1.2×10^{-7} | 5.7×10^{-8} | 1.6×10^{-6} |
| | 1 | 4.3×10^7 | - | 5.0×10^{-5} | 4.9×10^{-5} | 6.4×10^{-4} |
| | 10^2 | 6.7×10^5 | - | 8.4×10^{-3} | 1.2×10^{-2} | 1.1×10^{-1} |
| TŻO burst | 10^4 | 1.1×10^4 | 1.0×10^4 | 75 | - | 6.3×10^2 |
| | 10^6 | 2.0×10^2 | 1.5×10^6 | 6.4×10^3 | - | 5.3×10^4 |

(i.e., signal duration of months to years and accretion rates $10^{-4}M_\odot \text{ yr}^{-1} \leq \dot{M} \leq 10^4M_\odot \text{ yr}^{-1}$).

4.1. TŻO bursts

In order to investigate the neutrino detection prospects, we consider operative water-Cherenkov neutrino detectors, such as the IceCube Neutrino Observatory (Abbasi et al. 2011) and Super-Kamiokande (Abe et al. 2016; Kashiwagi et al. 2024), as well as the next-generation Hyper-Kamiokande (Abe et al. 2018) which is expected to have increased sensitivity with respect to Super-Kamiokande due to the larger fiducial volume. As detailed in Appendix B, neutrinos are mainly detected via inverse beta decay (IBD, $\bar{\nu}_e + p \rightarrow n + e^+$). However, quasi-elastic scattering of electron (anti)neutrinos on oxygen ($\nu_e + {}^{16}\text{O} \rightarrow e^- + X$ and $\bar{\nu}_e + {}^{16}\text{O} \rightarrow e^+ + X$, where X denotes the final state nucleus) and elastic scattering of all flavor (anti)neutrinos on electrons ($\nu_\alpha + e^- \rightarrow \nu_\alpha + e^-$ and $\bar{\nu}_\alpha + e^- \rightarrow \bar{\nu}_\alpha + e^-$, for each flavor α) also contribute to the signal event rate.

Figure 3 (left panel) displays the sensitivity of IceCube, Super-Kamiokande, and Hyper-Kamiokande to detect neutrinos from TŻO bursts at a distance D from Earth and lasting for Δt_ν (note that the difference in the event rate between Super-Kamiokande and Hyper-Kamiokande is mainly a scaling factor due to the roughly ten times larger effective volume of Hyper-Kamiokande). In Fig. 3, for $\dot{M} = 10^4M_\odot \text{ yr}^{-1}$ and $10^6M_\odot \text{ yr}^{-1}$, we highlight in color the regions of the plane spanned by the TŻO distance from Earth and Δt_ν , where the signal-to-noise ratio would be larger than 3 ($S/\sqrt{S+B} > 3$, where S and B denote the number of signal and background events, respectively); this corresponds to the 3σ exclusion of the signal hypothesis in the absence of additional systematic uncertainties.

IceCube has a larger effective area than Super-Kamiokande (and Hyper-Kamiokande), therefore it can

collect a larger number of signal events. Nevertheless, it features a significant rate of background events (Abbasi et al. 2011, $1.5 \times 10^6 \text{ s}^{-1}$), with respect to Super-Kamiokande, which has negligible backgrounds for burst-like searches. As a consequence, Super-Kamiokande has a better sensitivity to TŻOs at larger distances (cf. Fig. 3 and Table 1) than IceCube. Moreover, Super-Kamiokande allows to reconstruct spectral energy information of the detected neutrinos, not available at IceCube.

The left panel of Fig. 3 shows that, for TŻO bursts with accretion rate equal to $10^6M_\odot \text{ yr}^{-1}$ ($10^4M_\odot \text{ yr}^{-1}$), we would be able to detect neutrinos up to the Small Magellanic Cloud for $\Delta t_\nu \gtrsim 0.5 \text{ s}$ ($\Delta t_\nu \gtrsim 100 \text{ s}$). Such detection prospects clearly illustrate the potential of existing neutrino observatories of monitoring TŻOs in a larger fraction of the local Universe than future gravitational waves detectors would be able to do. In fact, the sensitivity of the latter is expected to be limited to Galactic events (DeMarchi et al. 2021; Renzo et al. 2021).

4.2. Steady TŻOs

If accretion is sustained for relatively long periods of time (i.e., at least several hours), a different detection strategy at neutrino observatories should be employed. In fact, to capture a steady neutrino signal lasting for months to years, we should search for an excess of neutrino events over background for a given time window. To this purpose, the neutrino telescopes Super-Kamiokande, JUNO (An et al. 2016), and Hyper-Kamiokande would lead the detection efforts.

We focus on the potential of Super-Kamiokande loaded with Gadolinium to enhance its sensitivity to electron antineutrinos (Abe et al. 2022, 2024). Our projections assume that Hyper-Kamiokande would have a similar setup, while being larger in size. By adopt-

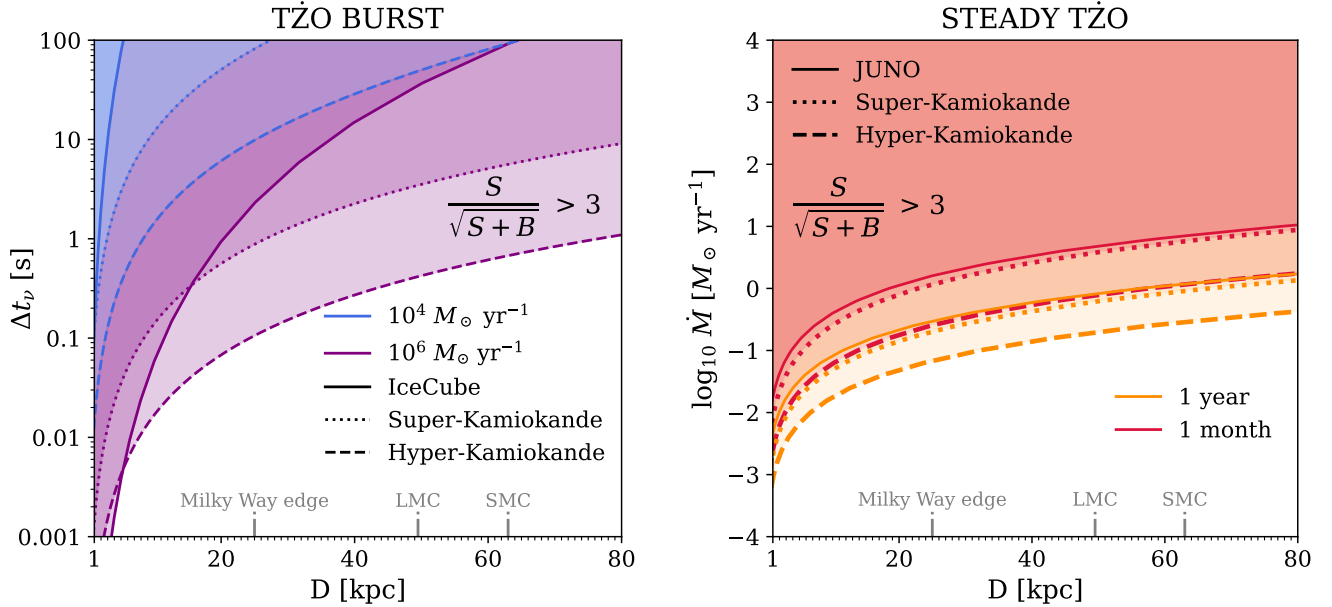


Figure 3. Detection prospects of neutrinos from TZO bursts. *Left panel:* Sensitivity of neutrino detection from TZO bursts detected by IceCube (solid lines), Super-Kamiokande (dotted lines) and Hyper-Kamiokande (dashed lines) in the plane spanned by the source distance from Earth and the signal duration. In order to guide the eye, the Milky Way edge is marked on the x-axis, together with the Large and Small Magellanic Cloud (LMC and SMC, respectively). The shaded regions correspond to a signal-to-noise ratio larger than 3, for constant accretion rates of $10^4 M_\odot \text{ yr}^{-1}$ and $10^6 M_\odot \text{ yr}^{-1}$, in blue and purple, respectively. Super-Kamiokande (Hyper-Kamiokande) and IceCube are sensitive to neutrino bursts from TZO bursts, lasting for $\gtrsim \mathcal{O}(0.1)$ s, within our Galaxy and beyond the Small Magellanic Cloud. *Right panel:* Same as left panel, but for steady TZOs detected by Super-Kamiokande (dotted lines), JUNO (solid lines), and Hyper-Kamiokande (dashed lines). The orange and red bands correspond to data-taking windows of one year and one month, respectively. Super-Kamiokande and JUNO should be sensitive to the neutrino emission from steady TZOs beyond the Small Magellanic Cloud for $\dot{M} \gtrsim 0.1 M_\odot \text{ yr}^{-1}$.

ing the same region of interest used for searches of the diffuse supernova neutrino background (DSNB), we could look for an electron antineutrino flux from TZO bursts through inverse beta decay in the energy window where the backgrounds are under control. Hence, we consider Super-Kamiokande and Hyper-Kamiokande with a detection efficiency of 55% (corresponding to water loaded with Gadolinium) in the energy window between 9.3 and 31.3 MeV, with a background rate of $1.0 \times 10^{-6} \text{ s}^{-1}/(100 \text{ kT})$ (Abe et al. 2021). As for JUNO, we assume a detection efficiency of 80% for energies between 12 and 30 MeV, with a background event rate of $1.4 \times 10^{-7} \text{ s}^{-1}/(17 \text{ kT})$ (Abusleme et al. 2022). We refer the reader to Appendix B for additional details.

Figure 3 (right panel) displays the sensitivity of Super-Kamiokande, Hyper-Kamiokande, and JUNO in the plane spanned by the mass accretion rate and the distance of the source from Earth for two different time windows of data taking of one month (in red) and one year (in orange), respectively. As for the case of TZO bursts in the left panel of the same figure, we highlight in color the regions of the parameter space with a signal-to-noise ratio larger than 3. We can see that neutrino

from TZO bursts with accretion rates larger than $0.1 M_\odot \text{ yr}^{-1}$ can be detected at Super-Kamiokande and JUNO, even if the source is located beyond the Small Magellanic Cloud. Table 1 also summarizes the signal event rates expected for steady TZOs.

4.3. Can we rely on neutrino detection to identify TZO candidates?

Figure 1 indicates that, among the TZO candidates, VX Sgr (Tabernero et al. 2021) is at $\sim 1.5\text{--}1.7$ kpc. If its accretion rate is $\gtrsim 10^{-2} M_\odot \text{ yr}^{-1}$, neutrino searches guided by Super-Kamiokande, IceCube, and soon by JUNO would be able to identify this source as a TZO, since large neutrino event statistics should be observed, independent of the theoretical uncertainties on the source properties. On the other hand, if dedicated searches should not lead to any positive neutrino detection, this may be an indication that VX Sgr is not a TZO or its accretion rate is so low that neutrino production is inefficient.

As for HV 2112 (Levesque et al. 2014) and HV 11417 (Beasor et al. 2018), these sources are at ~ 60 kpc from Earth. We could adopt Super-Kamiokande

and IceCube to test whether these sources have an accretion rate around $10^6 M_\odot \text{ yr}^{-1}$ or larger. If these sources should be steady TŻOs, then one year of neutrino data taking with Super-Kamiokande (JUNO) would constrain accretion rates above $0.9 M_\odot \text{ yr}^{-1}$ ($1.2 M_\odot \text{ yr}^{-1}$).

As for the potential TŻO progenitors shown in Fig. 1, the vast majority of such sources (Ge et al. 2024; DeMarchi et al. 2021; Manikantan et al. 2024) is located within 10 kpc from Earth. This implies that, if these or similar sources were to become steady TŻOs, we should expect to detect a cumulative flux of neutrinos with existing (or soon-to-be operative) detectors for accretion rates $\gtrsim 10^{-2} M_\odot \text{ yr}^{-1}$ after one year of data taking. If, instead, these candidates should evolve into TŻO bursts, then we would detect their neutrino emission for $\dot{M} \gtrsim 10^5 M_\odot \text{ yr}^{-1}$.

There may be additional undetected candidates within the Local Group that could undergo a merger in the near future. Most of our current understanding of such events comes from low-mass stellar mergers in the Galaxy, such as the archetypal luminous red nova V1309 Sco (Tylenda et al. 2011). However, for the more massive TŻO progenitors, the merger has been predicted to result in a luminous merger-driven explosion (Schröder et al. 2020). One promising prospect for the electromagnetic detection of such mergers is, for example, the Rubin Observatory/LSST (LSST Science Collaboration et al. 2009). A coincident detection of a luminous explosion with neutrino emission could provide compelling evidence of the formation of TŻOs. In addition, it can shed light on the physics behind the collapse of a neutron star into a black hole, as well as on the formation of TŻOs with a low-mass thin-envelope (Everson et al. 2024).

Given that Super-Kamiokande is currently taking data and JUNO is expected to become operative within the next year, we urge to carry out searches of neutrinos from TŻOs. Such targeted programs, for burst-like and steady TŻOs, will be crucial to assess the nature of existing TŻO candidates, eventually providing crucial insight on the nature of the source core that the electromagnetic data cannot probe. This is especially timely in light of the fact that any gravitational wave signal from TŻOs could be detected only with next-generation detectors (DeMarchi et al. 2021; Renzo et al. 2021).

5. DIFFUSE NEUTRINO FLUX FROM TŻOS

The cumulative neutrino flux from all past core collapses constitutes the diffuse supernova neutrino background (Ando et al. 2023, DSNB). Analogously, the diffuse neutrino flux from all TŻOs should permeate the Universe, partially overlapping in energy with the DSNB and with the diffuse neutrino flux from neutron-

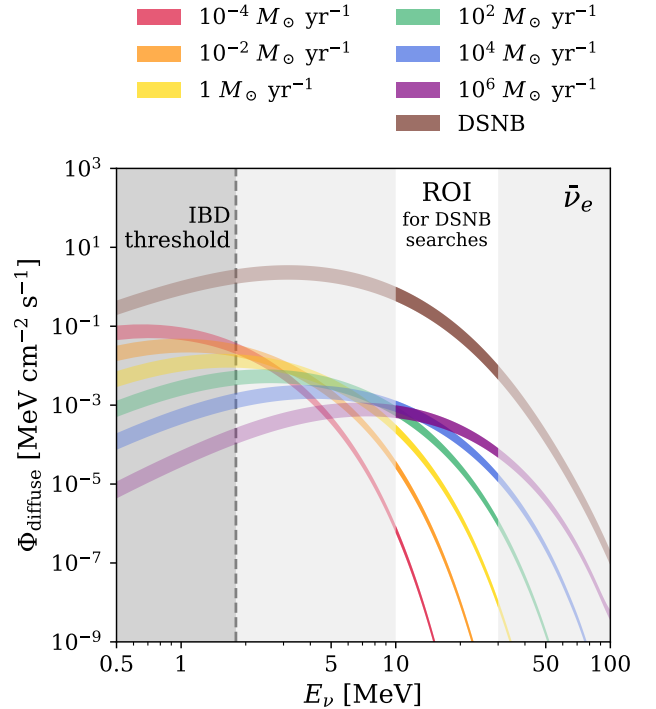


Figure 4. Diffuse flux of electron antineutrinos from TŻOs as a function of the neutrino energy, assuming that all TŻOs accrete at the same rate. The colored bands correspond to the accretion rates considered in this work, and the width of each band represents the uncertainty on the local rate of TŻO (see Eq. 3). The region of interest (ROI) for detection coincides with the one from the DSNB searches (i.e., the white vertical band between 10 and 30 MeV). The energy threshold for inverse beta decay (IBD, the most promising detection channel) is marked by the dashed line at 1.8 MeV. For comparison, the brown band represents the DSNB computed as in Martínez-Miravé et al. (2024). The diffuse flux of electron antineutrinos from TŻOs is significantly smaller than the DSNB, and it is therefore undetectable.

star mergers, which is expected to be lower than the DSNB (Tamborra 2024).

This diffuse TŻO neutrino flux is given by

$$\Phi_{\text{diffuse}}(E_\nu) = \int_0^{z_{\text{max}}} dz \frac{\mathcal{R}_{\text{TŻO}}(z, \dot{M})}{H(z)} \left. \frac{dN_\nu}{dE_\nu} \right|_{E_\nu(1+z)}, \quad (2)$$

where $H(z)$ is the Hubble parameter, $\mathcal{R}_{\text{TŻO}}(z, \dot{M})$ is the cosmic rate of TŻOs at a given redshift z and for an accretion rate \dot{M} , and dN_ν/dE_ν is the neutrino energy distribution from a TŻO (with duration given by Eq. 1 and where we consider a constant mass accretion rate such that $\Delta m = 1 M_\odot$). Moreover, we assume that the duration of the neutrino emission from a TŻO is much shorter than the cosmological timescales.

We assume that the rate of TŻOs follows the star formation history, $\dot{\rho}_*$, parametrized as in [Horiuchi et al. \(2009\)](#). We take the local rate of TŻOs to be $\xi_0 = 10^{-4} M_\odot^{-1}$ ([Nathaniel et al. 2024](#)). Then, the cosmic rate is

$$\mathcal{R}_{\text{TŻO}}(z, \dot{M}) = \xi_0 \dot{\rho}_*(z) \delta(\dot{M} - \dot{M}_0), \quad (3)$$

where δ denotes the Dirac delta distribution. We take into account the contribution from TŻOs up to redshift $z_{\text{max}} = 5$, since the contribution from larger redshifts should only matter for neutrinos with energy below 1 MeV, whose detection prospects are not optimal. In addition, the equation above assumes that the accretion rate is the same for all TŻO in the Universe (\dot{M}_0).

Current searches for a flux of neutrinos of astrophysical origin in the energy range of interest (i.e., 10–100 MeV) focus on electron antineutrino detection through inverse beta decay. [Figure 4](#) displays the predicted diffuse flux of electron antineutrinos for our selected accretion rates together with the DSNB for comparison. The white vertical band marks the region of interest (ROI) for DSNB searches between 10 and 30 MeV ([Vitagliano et al. 2020](#)), and the dashed vertical line indicates the detection threshold for inverse beta decay. Even under the assumption that all TŻOs have large accretion rates, the diffuse neutrino emission should be at least two orders of magnitude lower than the DSNB, hindering the detection of the diffuse neutrino emission from TŻOs.

6. CONCLUSIONS

In this *Letter*, we compute the neutrino emission from Thorne-Żytkow Objects (TŻOs) and explore their detection prospects. We rely on a steady spherically-symmetric model of the source, assuming a constant accretion rate varying between $10^{-4} M_\odot \text{ yr}^{-1}$ and $10^6 M_\odot \text{ yr}^{-1}$. If hypercritical (super-Eddington) accretion rates are achieved, we find that the high temperature and electron number density in the proximity of the neutron star lead to a sizeable production of thermal neutrinos, mainly via electron-positron pair annihilation. For the accretion-rate range considered in this work, the expected neutrino flux peaks between 2 and 20 MeV, varying approximately 7 orders of magnitude in amplitude.

The duration of the expected neutrino signal could largely vary between a few milliseconds and $\mathcal{O}(10^{11})$ s. Hence, in order to investigate the detection chances of TŻO neutrinos, we distinguish between “TŻO bursts” (if the accretion rate is $\gtrsim 10^4 M_\odot \text{ yr}^{-1}$) and “steady TŻOs” (for accretion rates that are $\lesssim 10^4 M_\odot \text{ yr}^{-1}$). The IceCube and Super-Kamiokande neutrino observatories are already sensitive to TŻO bursts, even beyond the Small

Magellanic Cloud (i.e., $\gtrsim 60$ kpc), if the burst duration should be larger than a few seconds. Super-Kamiokande and the soon-to-be operative JUNO can extend the sensitivity to accretion rates as low as $1 M_\odot \text{ yr}^{-1}$, if sustained for periods of time ranging from a month to years. In the near future, the Hyper-Kamiokande neutrino observatory will further strengthen these detection prospects.

Intriguingly, Super-Kamiokande and IceCube could already test the neutrino emission from existing TŻO candidates. As for the nearby source, VX Sgr, located at 1.5–1.7 kpc, if this is a TŻO with an accretion rate larger than $10^{-3} M_\odot \text{ yr}^{-1}$, targeted searches should detect neutrinos with large statistics, independent of the uncertainties on the source model. The candidates HV 2112 and HV 11417 are located at about 60 kpc from Earth. Super-Kamiokande would be able to detect neutrinos from these sources, if they are TŻOs with an accretion rate larger than $0.5 M_\odot \text{ yr}^{-1}$.

Such encouraging neutrino detection prospects should motivate the establishment of dedicated searches to test neutrino emission from TŻOs with existing and upcoming neutrino telescopes. This is especially timely, since neutrinos have the unique potential to assess the nature of TŻO candidates. In fact, the electromagnetic signal does not allow us to discriminate whether a neutron star is hosted at the core of such objects, and their gravitational wave emission could only be tested by upcoming gravitational wave detectors. The diffuse emission of neutrinos coming from all TŻOs in our Universe falls in the same energy region of the diffuse supernova neutrino background and it is negligible with respect to the latter.

This work highlights the relevance of neutrinos as key messengers to ascertain the existence of TŻOs in our Galaxy, and in certain cases even in the Local Group. While we employ a simplified model to compute the neutrino emission from these sources, our work highlights the importance of carrying out follow-up work on the neutrino signals from TŻOs and lays down specific detection strategies to test the nature of TŻO candidates and their properties. All in all, complementing ongoing observational efforts across wavelengths, neutrino searches would be of pivotal importance to probe this population of exotic stellar objects.

ACKNOWLEDGMENTS

This project has received support from the Villum Foundation (Project No. 13164), the Carlsberg Foundation (CF18-0183), and the Deutsche Forschungsgemeinschaft through Sonderforschungsbereich SFB 1258 “Neutrinos and Dark Matter in Astro- and Particle Physics”

(NDM). Part of this work was performed at Aspen Center for Physics, which is supported by National Science Foundation grant PHY-2210452. The Tycho supercom-

puter hosted at the SCIENCE HPC Center at the University of Copenhagen was used for supporting the numerical simulations presented in this work.

APPENDIX

A. SOURCE MODELLING AND THERMAL NEUTRINO PRODUCTION

In this appendix, we introduce the steady and spherically-symmetric model employed for TŻOs. Moreover, we outline the main reaction channels adopted to compute the neutrino emission from TŻOs and the approach we have used to compute flavor conversion.

A.1. Steady and spherically-symmetric TŻO model

In order to model the neutrino emission from TŻOs, we follow the analytical approach presented in [Chevalier \(1989\)](#). To this purpose, we consider a steady and spherically-symmetric inflow of shocked gas surrounding the neutron star. This approach also assumes that the fluid velocity is subsonic and the postshock flow is adiabatic. The first assumption is not valid in the vicinity of the shock wave; whereas the second assumption relies on the fact that neutrino energy losses are not negligible in the proximity of the neutron star. Within this framework, we derive the density and temperature profiles of the TŻO envelope. Moreover, for simplicity, we consider a constant electron fraction, $Y_e = 0.5$.

As for the neutron-star properties, we assume a mass of $M_{\text{NS}} = 1.4 M_\odot$ and a radius $r_{\text{NS}} = 10$ km, with constant density and temperature within r_{NS} , equal to the temperature at its surface. Note that the density and temperature profiles in the envelope are negligibly affected by such assumptions. The baryon density profile is

$$\rho(r) = \begin{cases} \frac{3M_{\text{NS}}}{4\pi r_{\text{NS}}^3} & r \leq r_{\text{NS}} \\ \rho_{\text{sh}} \left(\frac{r}{r_{\text{sh}}}\right)^{-3} & r_{\text{NS}} < r \leq r_{\text{sh}} \\ \frac{\dot{M}}{4\pi r_{\text{sh}}^2 v_{\text{ff}}(r)} & r > r_{\text{sh}} \end{cases}, \quad (\text{A1})$$

where we define the characteristic density (ρ_{sh}) and the free-fall velocity (v_{ff}) as

$$\rho_{\text{sh}} = 7 \frac{\dot{M}}{4\pi r_{\text{sh}}^2 v_{\text{ff}}(r_{\text{sh}})} \quad \text{and} \quad v_{\text{ff}}(r) = \sqrt{\frac{2GM_{\text{NS}}}{r}}. \quad (\text{A2})$$

Here, G is the gravitational constant, \dot{M} is the accretion rate, r_{sh} indicates the location of the accretion-shock radius ([Chevalier 1989](#)):

$$r_{\text{sh}} = 3.6 \times 10^8 \left(\frac{\dot{M}}{M_\odot \text{ yr}^{-1}}\right)^{-4/10} \left(\frac{r_{\text{NS}}}{10^6 \text{ cm}}\right)^{8/5} \left(\frac{M_{\text{NS}}}{1.4 M_\odot}\right)^{-1/15}. \quad (\text{A3})$$

Similarly, the temperature profile scales as

$$T(r) = \begin{cases} T_{\text{NS}} & r \leq r_{\text{NS}} \\ T_{\text{sh}} \left(\frac{r}{r_{\text{sh}}}\right)^{-1} & r_{\text{NS}} < r \leq r_{\text{sh}} \\ T_{\text{sh}} \left(\frac{\rho(r)}{\rho_{\text{sh}}}\right)^{1/3} & r > r_{\text{sh}} \end{cases}, \quad (\text{A4})$$

where the temperature at the shock front (T_{sh}) and at the neutron-star surface (T_{NS}) are given by

$$T_{\text{sh}} = \left(\frac{6 \dot{M} v_{\text{ff}}(r_{\text{sh}})}{7 \cdot 4\pi r_{\text{sh}}^2 a}\right)^{1/4} \quad \text{and} \quad T_{\text{NS}} = T_{\text{sh}} \frac{r_{\text{sh}}}{r_{\text{NS}}}, \quad (\text{A5})$$

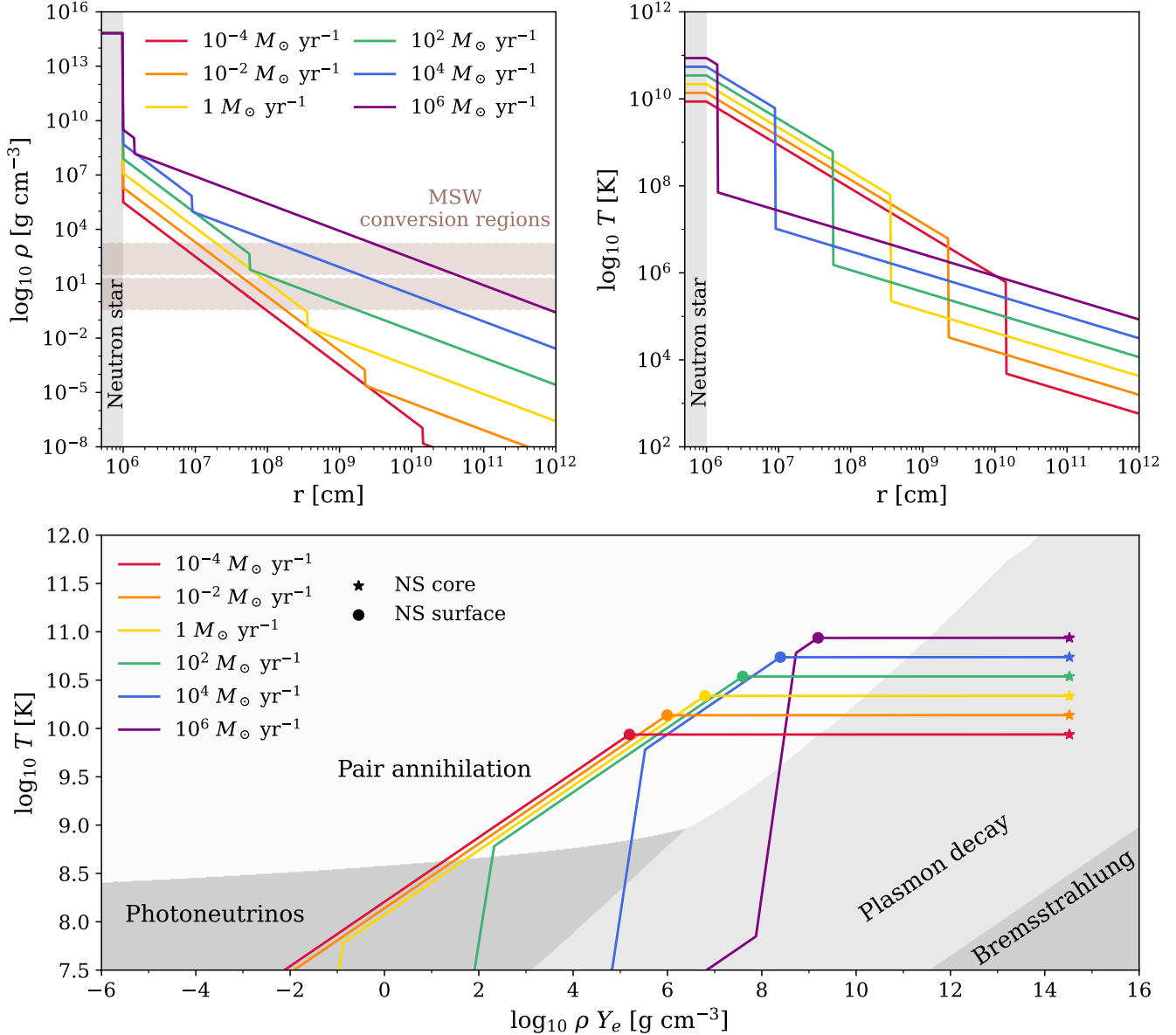


Figure 5. *Top panels:* Radial evolution of the baryon density on the left and temperature on the right, for different accretion rates. The brown horizontal bands in the top left panel highlight the regions where MSW flavor conversion is expected to take place for the solar and atmospheric neutrino mass differences and $E_{\nu} \in [2, 100]$ MeV. *Bottom panel:* Dominant mechanisms for thermal neutrino production in the plane spanned by the electron density and temperature of the medium. The shaded regions indicate the dominant processes: electron-positron pair annihilation, plasmon decay, photoneutrino production, and bremsstrahlung (Dicus 1972; Dutta et al. 2004; Braaten & Segel 1993; Guo & Qian 2016; Haft et al. 1994). The colored lines correspond to the density and temperature profiles for different accretion rates from 10^{-4} to $10^6 M_{\odot} \text{ yr}^{-1}$. The star-shaped markers indicate the characteristic temperature and density of the neutron star (assumed to be constant for simplicity); the point-like markers signal the thermodynamical quantities right outside of the neutron star (assuming a sharp boundary). Neutrino emission is dominated by pair annihilation in the surroundings of the neutron star at the core of the TZO.

with $a = 4\sigma/c$, σ is the Stefan–Boltzmann constant, and c is the speed of light. Given the wide range of accretion rates explored in this paper, the temperatures at the surface of the neutron star can vary between 10^{10} and 10^{11} K. As for the baryon density at the innermost layer of the envelope, it can vary between 10^4 g cm⁻³ and 10^9 g cm⁻³. The resulting temperature and density profiles for different mass accretion rates are plotted in the top panels of Fig. 5.

A.2. Neutrino emission rates

The neutrino emission rate through pair annihilation ($e^+ + e^- \rightarrow \nu + \bar{\nu}$, [Dicus \(1972\)](#)) and photoneutrino production ($\gamma + e^- \rightarrow e^- + \nu + \bar{\nu}$, [Dutta et al. \(2004\)](#)) grow with temperature. The pair annihilation rate also presents a mild growth as the electron density increases. As shown in the bottom panel of [Fig. 5](#), neutrino emission is dominated by pair annihilation in the vicinity of the neutron star and photoneutrino production at smaller densities. In the neutron star, the main neutrino production channel is plasmon decay ($\gamma^* \rightarrow \nu + \bar{\nu}$, [Braaten & Segel \(1993\)](#)). However, due to the very high densities [$\mathcal{O}(10^{14})$ g cm $^{-3}$], we find that absorption is so large that the neutron star can be safely treated as opaque to neutrinos.

In the absence of flavor conversion, the neutrino flux at Earth for a given neutrino of flavor α is defined as

$$\frac{d^2\Phi_{\nu\alpha,0}}{dE_\nu dt} = \int dr \frac{r^2}{2D^2} \left[1 + \sqrt{1 - \frac{r_{\text{NS}}^2}{r^2}} \right] R_{\nu\alpha}(\tilde{E}(r), \rho(r), T(r)), \quad (\text{A6})$$

which depends on the neutrino emission rate for given temperature and baryon density. The energy at which neutrinos are produced and detected are \tilde{E} and E_ν , respectively, with $\tilde{E} = E_\nu / \sqrt{1 - 2GM_{\text{NS}}/r}$. This redshift correction on the neutrino energy is due to the curved spacetime in the proximity of the neutron star. We have also included the geometric factor $1/2 \left[1 + \sqrt{1 - (r_{\text{NS}}/r)^2} \right]$, which accounts for the fact that neutrino absorption is negligible in the envelope outside the neutron star, but the neutron star is completely opaque to neutrinos.

A.3. Neutrino flavor conversion

Lepton number conservation ensures that the same amount of neutrinos and antineutrinos of each flavor are produced. Electron flavor neutrinos are produced via charged and neutral weak interactions, whereas non-electron neutrinos are produced only through neutral current interactions. Hence, the fraction of electron flavor neutrino-antineutrino pairs is larger than the one of each non-electron flavor neutrino-antineutrino pair.

Neutrinos are mainly produced in a region extending for several tens of km outside the neutron star. When traveling outwards, they experience Mikheyev–Smirnov–Wolfenstein (MSW) resonant flavor conversion ([Wolfenstein 1978](#); [Mikheyev & Smirnov 1985](#)) when they cross the baryon density at $\sim 10^2$ – 10^3 g cm $^{-3}$ and ~ 1 – 10 g cm $^{-3}$, as illustrated in the top left panel of [Fig. 5](#). We have tested that, due to the source properties, neutrino flavor evolution in the TŻO envelope is adiabatic. Then, taking into account the loss of coherence for neutrinos en route to Earth, as illustrated in [Dighe & Smirnov \(2000\)](#), we obtain the (anti)neutrino fluxes at Earth. In this work, the three-flavor neutrino oscillation parameters are set as in [de Salas et al. \(2021\)](#).

B. NEUTRINO EVENT RATE IN EXISTING AND UPCOMING NEUTRINO TELESCOPES

In this appendix, we discuss how to compute the event rate of neutrinos from TŻOs in existing neutrino telescopes, such as IceCube and Super-Kamiokande, as well as in the upcoming Hyper-Kamiokande and JUNO.

B.1. IceCube Neutrino Observatory

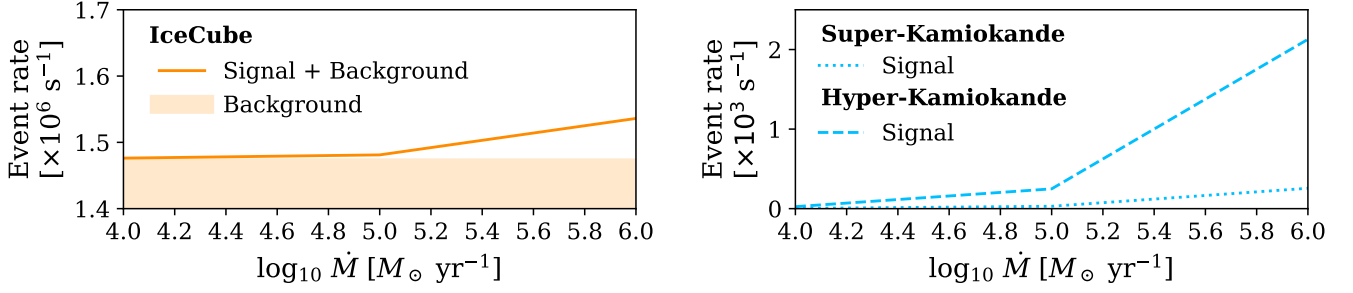
The IceCube Neutrino Observatory is a water-Cherenkov detector located at the South Pole and consisting of 5160 digital optical modules (DOMs). IceCube is expected to be sensitive to neutrinos from TŻOs via (i) the inverse beta decay channel ($\bar{\nu}_e + p \rightarrow e^+ + n$); (ii) the elastic scattering of neutrinos of all flavors on electrons ($\nu_\alpha + e^- \rightarrow \nu_\alpha + e^-$ and $\bar{\nu}_\alpha + e^- \rightarrow \bar{\nu}_\alpha + e^-$, with $\alpha = e, \mu, \tau$); (iii) the quasi-elastic scattering of electron neutrinos on oxygen ($\nu_e + {}^{16}\text{O} \rightarrow e^- + X$ and $\bar{\nu}_e + {}^{16}\text{O} \rightarrow e^+ + X$, where X denotes a different final state nucleus) by measuring the Cherenkov photons radiated by the final-state electrons and positrons.

Following [Abbasi et al. \(2011\)](#), we compute the hit count per DOM for each reaction channel as

$$r_{\text{IC}} = n_{\text{target}} \int dE_e \int dE_\nu \frac{d\sigma(E_\nu, E_e)}{dE_e} N_\gamma(E_e) V_\gamma^{\text{eff}} \Phi(E_\nu), \quad (\text{B7})$$

where n_{target} is the number density of targets for a density of 0.92 g cm $^{-3}$. The effective volume for a single photon is $V_\gamma^{\text{eff}} = 0.163$ and the energy-dependent number of radiated photons as a function of the electron or positron kinetic energy (E_e) is $N_\gamma(E_e) \simeq 178 E_e/\text{MeV}$. Finally, $d\sigma/dE_e$ denotes the cross-section for the detection channels listed above. Such cross-sections have been implemented following [Strumia & Vissani \(2003\)](#); [Ricciardi et al. \(2022\)](#); [Marciano & Parsa \(2003\)](#); [Kolbe et al. \(2002\)](#).

TŻO BURST



STEADY TŻO

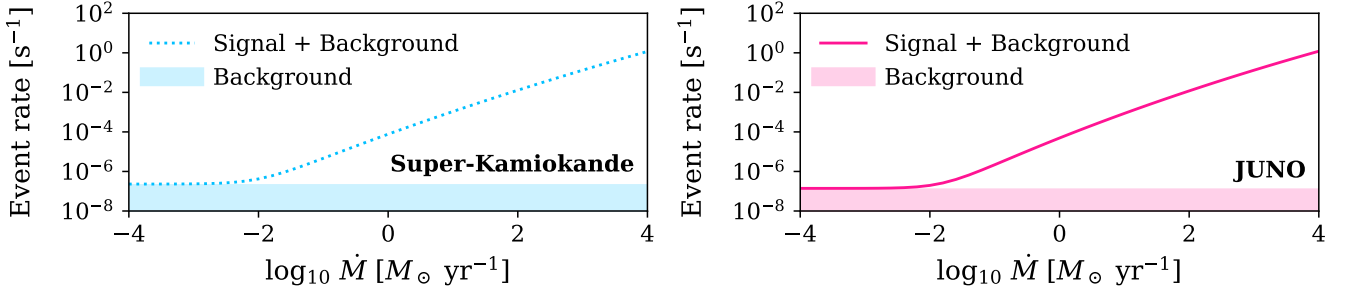


Figure 6. *Top panels:* Expected event rate for a TŻO burst at 5 kpc from Earth for IceCube (left panel), Super-Kamiokande (dotted line, right panel), and Hyper-Kamiokande (dashed line, right panel). The IceCube background rate is shown as a shaded band. For Super-Kamiokande (Hyper-Kamiokande), the background rate is 10^{-2} s^{-1} (0.1 s^{-1}), and thus not displayed. *Bottom panels:* Expected event rate for a steady TŻOs at 5 kpc from Earth for Super-Kamiokande (left panel) and JUNO (right panel). The background rates are displayed as shaded bands. The total and background-only event rates for Hyper-Kamiokande are analogous to the ones shown for Super-Kamiokande, after accounting for the difference in fiducial volume of approximately one order of magnitude (and therefore not shown here).

Defining r as the sum of the hit count per DOM for all reaction channels, the expected event rate is

$$R_{\text{IC}} = N_{\text{DOM}} r \frac{0.87}{1 + r \tau}, \quad (\text{B8})$$

where $\tau \simeq 250 \text{ s}$ is the deadtime and $N_{\text{DOM}} = 5160$ is the number of DOMs. The signal event rate is to be compared with the rate of background events and shot-noise, that is $1.5 \times 10^6 \text{ s}^{-1}$ (Abbasi et al. 2011), see the top left panel of Fig. 6. The large background rate makes IceCube unsuitable for the search of steady MeV neutrino sources. Besides that, IceCube can measure the total rate but can not recover accurate information on the energy spectrum.

B.2. Super-Kamiokande and Hyper-Kamiokande

The water-Cherenkov detector Super-Kamiokande is sensitive to TŻO neutrinos via inverse beta decay, elastic scattering on electrons, and quasi-elastic scattering on oxygen, like IceCube. The event rate for each detection channel is

$$R_{\text{SK}}(t) = n_{\text{targets}} \varepsilon \int dE_e \int dE_\nu \frac{d\sigma(E_\nu, E_e)}{dE_e} \Phi(E_\nu), \quad (\text{B9})$$

and we consider a fiducial volume of 22.5 kT of water. Neutrino searches from TŻO bursts are basically background free (the background rate is 0.012 s^{-1} , generally much smaller than the expected signal event rate, c.f. Table 1). We assume perfect detection efficiency ($\varepsilon = 1$) for all detection channels.

For steady TŻOs, the detection efficiency is assumed to be $\varepsilon = 0.55$ (resulting from a 75% neutron-capture efficiency for 0.03% of Gadolinium-loaded water and 74% selection efficiency Abe et al. (2024)). The detection window is limited

to neutrino energies between 9.3 and 31.3 MeV. For steady TŽOs, we only consider inverse beta decay events. These searches need to account for the background events from reactor antineutrinos, atmospheric neutrinos, as well as spallation backgrounds, and the DSNB. These backgrounds are included following [Martínez-Miravé et al. \(2024\)](#) and references therein. In the future, Hyper-Kamiokande ([Abe et al. 2018](#)) will further improve the detection prospects explored for Super-Kamiokande, due to its larger fiducial volume (187 kT of water). We assume a simple scaling in detector size from Super-Kamiokande, following [Martínez-Miravé et al. \(2024\)](#). The expected event rates as functions of the accretion rates for TŽO bursts and steady TŽOs are shown in Fig. 6 for both Super-Kamiokande and Hyper-Kamiokande.

B.3. JUNO

The liquid-scintillator neutrino detector JUNO is expected to be operative within the next year. While the event statistics expected in Super-Kamiokande and IceCube from TŽO bursts is larger than the one achievable in JUNO, the latter would be suitable for searches of neutrinos from steady TŽOs. JUNO is expected to be sensitive to electron antineutrinos via the inverse beta decay channel, with an event rate given by:

$$R_{\text{JUNO}} = n_{\text{targets}} \varepsilon \int dE_e \int dE_\nu \frac{d\sigma_{\text{IBD}}(E_\nu, E_e)}{dE_e} \Phi_{\bar{\nu}_e}(E_\nu). \quad (\text{B10})$$

Here, the number of proton targets is $n_{\text{targets}} = 1.22 \times 10^{33}$, equivalent to 17 kT, and the detection efficiency is $\varepsilon = 0.8$ ([Abusleme et al. 2022](#)). The event rate depends on the electron antineutrino flux ($\Phi_{\bar{\nu}_e}$) and the inverse beta decay cross section (σ_{IBD}). The main backgrounds expected in JUNO are due to reactor antineutrinos, atmospheric neutrinos, spallation backgrounds, and the DSNB ([Abusleme et al. 2022](#)). We take such backgrounds into account following [Martínez-Miravé et al. \(2024\)](#). The event rate expected in JUNO for steady TŽOs is shown in Fig. 6 (bottom right panel) with the related background rates.

REFERENCES

- Abbasi, R., et al. 2011, *Astron. Astrophys.*, 535, A109, doi: [10.1051/0004-6361/201117810e](https://doi.org/10.1051/0004-6361/201117810e)
- Abe, K., et al. 2016, *Astropart. Phys.*, 81, 39, doi: [10.1016/j.astropartphys.2016.04.003](https://doi.org/10.1016/j.astropartphys.2016.04.003)
- . 2018. <https://arxiv.org/abs/1805.04163>
- . 2021, *Phys. Rev. D*, 104, 122002, doi: [10.1103/PhysRevD.104.122002](https://doi.org/10.1103/PhysRevD.104.122002)
- . 2022, *Nucl. Instrum. Meth. A*, 1027, 166248, doi: [10.1016/j.nima.2021.166248](https://doi.org/10.1016/j.nima.2021.166248)
- . 2024, *Nucl. Instrum. Meth. A*, 1065, 169480, doi: [10.1016/j.nima.2024.169480](https://doi.org/10.1016/j.nima.2024.169480)
- Abusleme, A., et al. 2022, *JCAP*, 10, 033, doi: [10.1088/1475-7516/2022/10/033](https://doi.org/10.1088/1475-7516/2022/10/033)
- An, F., et al. 2016, *J. Phys. G*, 43, 030401, doi: [10.1088/0954-3899/43/3/030401](https://doi.org/10.1088/0954-3899/43/3/030401)
- Ando, S., Ekanger, N., Horiuchi, S., & Koshio, Y. 2023, *Proceedings of the Japan Academy, Series B*, 99, 460, doi: [10.2183/pjab.99.026](https://doi.org/10.2183/pjab.99.026)
- Beasor, E. R., Davies, B., Cabrera-Ziri, I., & Hurst, G. 2018, *Mon. Roy. Astron. Soc.*, 479, 3101, doi: [10.1093/mnras/sty1744](https://doi.org/10.1093/mnras/sty1744)
- Biehle, G. T. 1994, *Astrophys. J.*, 420, 364, doi: [10.1086/173566](https://doi.org/10.1086/173566)
- Braaten, E., & Segel, D. 1993, *Phys. Rev. D*, 48, 1478, doi: [10.1103/PhysRevD.48.1478](https://doi.org/10.1103/PhysRevD.48.1478)
- Cannon, R. C. 1993, *Mon. Roy. Astron. Soc.*, 263, 817, doi: [10.1093/mnras/263.4.817](https://doi.org/10.1093/mnras/263.4.817)
- Cannon, R. C., Eggleton, P. P., Zytlow, A. N., & Podsiadlowski, P. 1992, *Astrophys. J.*, 386, 206, doi: [10.1086/171006](https://doi.org/10.1086/171006)
- Chevalier, R. A. 1989, *Astrophys. J.*, 346, 847, doi: [10.1086/168066](https://doi.org/10.1086/168066)
- . 1993, *Astrophys. J. Lett.*, 411, L33, doi: [10.1086/186905](https://doi.org/10.1086/186905)
- de Salas, P. F., Forero, D. V., Gariazzo, S., et al. 2021, *JHEP*, 02, 071, doi: [10.1007/JHEP02\(2021\)071](https://doi.org/10.1007/JHEP02(2021)071)
- DeMarchi, L., Sanders, J. R., & Levesque, E. M. 2021, *Astrophys. J.*, 911, 101, doi: [10.3847/1538-4357/abebe1](https://doi.org/10.3847/1538-4357/abebe1)
- Dicus, D. A. 1972, *Phys. Rev. D*, 6, 941, doi: [10.1103/PhysRevD.6.941](https://doi.org/10.1103/PhysRevD.6.941)
- Dighe, A. S., & Smirnov, A. Y. 2000, *Phys. Rev. D*, 62, 033007, doi: [10.1103/PhysRevD.62.033007](https://doi.org/10.1103/PhysRevD.62.033007)
- Dutta, S. I., Ratkovic, S., & Prakash, M. 2004, *Phys. Rev. D*, 69, 023005, doi: [10.1103/PhysRevD.69.023005](https://doi.org/10.1103/PhysRevD.69.023005)
- Everson, R. W., Hutchinson-Smith, T., Vigna-Gómez, A., & Ramirez-Ruiz, E. 2024, *Astrophys. J.*, 971, 132, doi: [10.3847/1538-4357/ad595e](https://doi.org/10.3847/1538-4357/ad595e)

- Farmer, R., Renzo, M., Götberg, Y., et al. 2023, *Mon. Roy. Astron. Soc.*, 524, 1692, doi: [10.1093/mnras/stad1977](https://doi.org/10.1093/mnras/stad1977)
- Fryer, C. L., Benz, W., & Herant, M. 1996, *Astrophys. J.*, 460, 801, doi: [10.1086/177011](https://doi.org/10.1086/177011)
- Ge, H., Tout, C. A., Chen, X., et al. 2024, *Astrophys. J.*, 975, 254, doi: [10.3847/1538-4357/ad7ea6](https://doi.org/10.3847/1538-4357/ad7ea6)
- Guo, G., & Qian, Y.-Z. 2016, *Phys. Rev. D*, 94, 043005, doi: [10.1103/PhysRevD.94.043005](https://doi.org/10.1103/PhysRevD.94.043005)
- Haft, M., Raffelt, G., & Weiss, A. 1994, *Astrophys. J.*, 425, 222, doi: [10.1086/173978](https://doi.org/10.1086/173978)
- Horiuchi, S., Beacom, J. F., & Dwek, E. 2009, *Phys. Rev. D*, 79, 083013, doi: [10.1103/PhysRevD.79.083013](https://doi.org/10.1103/PhysRevD.79.083013)
- Houck, J. C., & Chevalier, R. A. 1991, *Astrophys. J.*, 376, 234, doi: [10.1086/170272](https://doi.org/10.1086/170272)
- Hutchinson-Smith, T., Everson, R. W., Twum, A. A., et al. 2024, *Astrophys. J.*, 977, 196, doi: [10.3847/1538-4357/ad88f3](https://doi.org/10.3847/1538-4357/ad88f3)
- Kashiwagi, Y., et al. 2024, *Astrophys. J.*, 970, 93, doi: [10.3847/1538-4357/ad4d8e](https://doi.org/10.3847/1538-4357/ad4d8e)
- Kolbe, E., Langanke, K., & Vogel, P. 2002, *Phys. Rev. D*, 66, 013007, doi: [10.1103/PhysRevD.66.013007](https://doi.org/10.1103/PhysRevD.66.013007)
- Kuchner, M. J., Vakil, D., Smith, V. V., et al. 2002, in *Astronomical Society of the Pacific Conference Series*, Vol. 263, *Stellar Collisions, Mergers and their Consequences*, ed. M. M. Shara, 131
- Levesque, E. M., Massey, P., Zytzkow, A. N., & Morrell, N. 2014, *Mon. Roy. Astron. Soc.*, 443, L94, doi: [10.1093/mnrasl/slu080](https://doi.org/10.1093/mnrasl/slu080)
- LSST Science Collaboration, Abell, P. A., Allison, J., et al. 2009, arXiv e-prints, arXiv:0912.0201, doi: [10.48550/arXiv.0912.0201](https://doi.org/10.48550/arXiv.0912.0201)
- Manikantan, H., Kumar, M., Paul, B., & Rana, V. 2024, *Mon. Not. Roy. Astron. Soc.*, 527, 640, doi: [10.1093/mnras/stad3090](https://doi.org/10.1093/mnras/stad3090)
- Marciano, W. J., & Parsa, Z. 2003, *J. Phys. G*, 29, 2629, doi: [10.1088/0954-3899/29/11/013](https://doi.org/10.1088/0954-3899/29/11/013)
- Martínez-Miravé, P., Tamborra, I., Aloy, M. A., & Obergaulinger, M. 2024, *Phys. Rev. D*, 110, 103029, doi: [10.1103/PhysRevD.110.103029](https://doi.org/10.1103/PhysRevD.110.103029)
- Mikheyev, S. P., & Smirnov, A. Y. 1985, *Sov. J. Nucl. Phys.*, 42, 913
- Moran-Fraile, J., Schneider, F. R. N., Roepke, F. K., et al. 2023, *Astron. Astrophys.*, 672, A9, doi: [10.1051/0004-6361/202245109](https://doi.org/10.1051/0004-6361/202245109)
- Nathaniel, K., Vigna-Gómez, A., Grichener, A., et al. 2024. <https://arxiv.org/abs/2407.11680>
- Nava-Callejas, M., Cavecchi, Y., & Page, D. 2024, *RAS Techniques and Instruments*, 3, 800, doi: [10.1093/rasti/rzae055](https://doi.org/10.1093/rasti/rzae055)
- Nazin, S. N., & Postnov, K. A. 1995, *Astron. Astrophys.*, 303, 789. <https://arxiv.org/abs/astro-ph/9505025>
- O’Grady, A. J. G., Moriya, T. J., Renzo, M., & Vigna-Gómez, A. 2024. <https://arxiv.org/abs/2410.02896>
- O’Grady, A. J. G., Drout, M. R., Gaensler, B. M., et al. 2023, *Astrophys. J.*, 943, 18, doi: [10.3847/1538-4357/aca655](https://doi.org/10.3847/1538-4357/aca655)
- Podsiadlowski, P., Cannon, R. C., & Rees, M. J. 1995, *Mon. Roy. Astron. Soc.*, 274, 485, doi: [10.1093/mnras/274.2.485](https://doi.org/10.1093/mnras/274.2.485)
- Podsiadlowski, P., Cannon, R. C., & Rees, M. J. 1995, *Mon. Not. Roy. Astron. Soc.*, 274, 485, doi: [10.1093/mnras/274.2.485](https://doi.org/10.1093/mnras/274.2.485)
- Renzo, M., Callister, T., Chatziioannou, K., et al. 2021, *Astrophys. J.*, 919, 128, doi: [10.3847/1538-4357/ac1110](https://doi.org/10.3847/1538-4357/ac1110)
- Ricciardi, G., Vignaroli, N., & Vissani, F. 2022, *JHEP*, 08, 212, doi: [10.1007/JHEP08\(2022\)212](https://doi.org/10.1007/JHEP08(2022)212)
- Schröder, S. L., MacLeod, M., Loeb, A., Vigna-Gómez, A., & Mandel, I. 2020, *Astrophys. J.*, 892, 13, doi: [10.3847/1538-4357/ab7014](https://doi.org/10.3847/1538-4357/ab7014)
- Strumia, A., & Vissani, F. 2003, *Phys. Lett. B*, 564, 42, doi: [10.1016/S0370-2693\(03\)00616-6](https://doi.org/10.1016/S0370-2693(03)00616-6)
- Taberner, H. M., Dorda, R., Negueruela, I., & Marfil, E. 2021, *Astron. Astrophys.*, 646, A98, doi: [10.1051/0004-6361/202039236](https://doi.org/10.1051/0004-6361/202039236)
- Tamborra, I. 2024. <https://arxiv.org/abs/2412.09699>
- Thorne, K. S., & Zytzkow, A. N. 1975, *Astrophys. J. Lett.*, 199, L19, doi: [10.1086/181839](https://doi.org/10.1086/181839)
- . 1977, *Astrophys. J.*, 212, 832, doi: [10.1086/155109](https://doi.org/10.1086/155109)
- Tylenda, R., Hajduk, M., Kamiński, T., et al. 2011, *Astron. Astrophys.*, 528, A114, doi: [10.1051/0004-6361/201016221](https://doi.org/10.1051/0004-6361/201016221)
- Vitagliano, E., Tamborra, I., & Raffelt, G. 2020, *Rev. Mod. Phys.*, 92, 45006, doi: [10.1103/RevModPhys.92.045006](https://doi.org/10.1103/RevModPhys.92.045006)
- Wolfenstein, L. 1978, *Phys. Rev. D*, 17, 2369, doi: [10.1103/PhysRevD.17.2369](https://doi.org/10.1103/PhysRevD.17.2369)